processes

MDPI

Article

Numerical Simulation and Optimization of Polyacrylamide Solution Flow in a Polymer Injector Using an Improved Viscosity Constitutive Model

Qin Qian [1], Tengyu Li [2], Congkun Ren [1,*], Yantao Zhou [2], Chuanrui Che [1], Xuemei Zhang [1], Jiaxing Ma [1], Pengxu An [2] and Qiuyang Zhao [2,*]

[1] Research Institute of Petroleum Engineering Technology, SINOPEC Shengli Oilfield Company, Dongying 257000, China
[2] State Key Laboratory of Multiphase Flow in Power Engineering, Xi'an Jiaotong University, Xi'an 710049, China
* Correspondence: rencongkun.slyt@sinopec.com (C.R.); qyzhao@xjtu.edu.cn (Q.Z.)

Abstract

Previous numerical simulations of polymer injectors often rely on fixed-viscosity models, which fail to accurately capture the severe shear degradation of non-Newtonian fluids under high-shear throttling conditions. To address this limitation and enhance polymer flooding efficiency, this study proposes an improved Carreau–Yasuda viscosity constitutive model to precisely simulate the flow behavior of polyacrylamide (HPAM) solutions. A comprehensive computational fluid dynamics (CFD) model was developed and validated, showing a viscosity prediction error of less than 8.6% across a wide shear rate range (0.1–10,000 s^{-1}). Based on this dynamic rheological model, the internal flow channel of the injector was optimized, resulting in a novel spindle-type throttling unit. Simulation and field validation results demonstrate that the optimized structure achieves a significant pressure drop of 6.03 MPa at an injection flow rate of 96 m^3/d—representing a 65% improvement over traditional designs—while successfully maintaining a viscosity retention rate above 85%. This research overcomes the traditional design conflict between high pressure reduction and viscosity preservation, providing an accurate numerical framework and practical guidance for engineering high-flow, robust-throttling polymer injectors.

Keywords: polymer injector; polyacrylamide solution; non-Newtonian fluid; Carreau–Yasuda model; numerical simulation; structural optimization

Check for updates

Academic Editors: Hai Wang and Gang Hui

Received: 29 January 2026
Revised: 4 March 2026
Accepted: 6 March 2026
Published: 10 March 2026

Copyright: © 2026 by the authors. Licensee MDPI, Basel, Switzerland. This article is an open access article distributed under the terms and conditions of the Creative Commons Attribution (CC BY) license.

1. Introduction

Polymer flooding has emerged as one of the most widely applied and effective chemical Enhanced Oil Recovery (EOR) techniques in mature oilfields [1,2]. By increasing the viscosity of the injected fluid, polymer solutions significantly improve the mobility ratio and volumetric sweep efficiency [3]. However, in highly heterogeneous reservoirs, conventional continuous injection often leads to severe fingering effects [4,5]. To mitigate these interlayer conflicts and ensure precise fluid distribution across strata with varying permeabilities, layered polymer injection technology has been aggressively developed and deployed [6,7].

The polymer injector serves as the core equipment in this layered injection process. Its fundamental principle relies on utilizing the annular gap between the throttling core and the mandrel to achieve staged throttling and pressure reduction for high-viscosity polymer fluids. Despite its widespread application, a critical engineering bottleneck persists: to

achieve the high pressure drops required for deep formations, traditional injector designs inevitably induce extreme shear rates within the narrow throttling zones [8,9]. This excessive mechanical shear leads to the irreversible scission of polyacrylamide (HPAM) molecular chains [10,11], causing a dramatic loss in apparent viscosity and directly impairing the ultimate oil displacement efficiency. Extensive research has been conducted to optimize the throttling tooth profile to balance pressure reduction and shear intensity. However, previous numerical simulations of polymer injectors predominantly relied on fixed-viscosity models or simplified non-Newtonian frameworks (such as the standard power-law model) [12–14].

These conventional models fail to accurately capture the highly nonlinear, dynamic evolution of polymer apparent viscosity under extreme shear rate variations, particularly when shear rates exceed 1000 s^{-1}. Consequently, the existing studies have been unable to effectively resolve the core conflict between "achieving a high pressure drop" and "maintaining high viscosity retention", as they lack a reliable theoretical basis to precisely regulate the local shear field.

To address the shortcomings of previous research, this study introduces a comprehensive structural optimization approach grounded in an advanced rheological framework. The primary innovation of this research lies in the establishment of an improved Carreau–Yasuda viscosity constitutive equation, derived from transient rheological experiments covering an exceptionally wide shear rate range (10^{-1} to 10^{4} s^{-1}). By dynamically coupling this accurate constitutive model into computational fluid dynamics (CFD) simulations, we effectively capture the real-time response between shear rate and viscosity. Ultimately, this study proposes a novel spindle-shaped throttling unit, aiming to provide a robust, scientifically grounded solution that simultaneously maximizes pressure-reducing performance and preserves polymer viscosity, thereby offering significant practical value for EOR engineering applications.

2. Materials and Methods

2.1. Rheological Property Testing

In the experiment, the polymer used was partially hydrolyzed polyacrylamide (HPAM), appearing as white powdery crystals. To facilitate the reproducibility of this study, it is specified that the HPAM was supplied by SNF Floerger (Andrezieux, France), a widely recognized manufacturer for chemical EOR applications. The polymer has a weight-average molecular weight of 20×10^6 Da and a degree of hydrolysis of 25%.

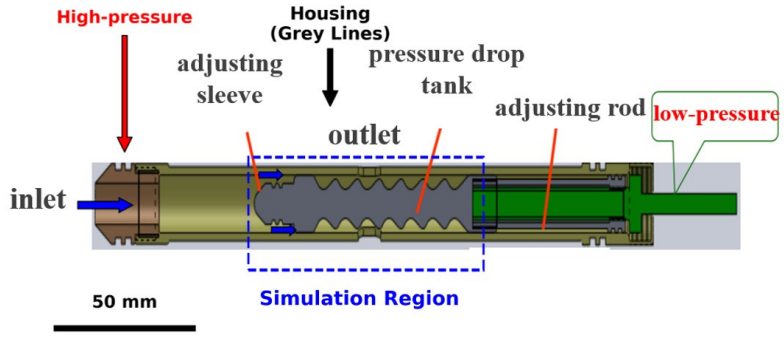
A specific mass of deionized water was accurately weighed in a 300 mL beaker. Furthermore, it should be noted that deionized water was intentionally selected as the solvent for solution preparation in this fundamental phase of the study. While field applications typically involve formation water, the use of deionized water effectively isolates the baseline rheological behavior of the HPAM solution, avoiding the complex electrostatic shielding effects and viscosity fluctuations introduced by multivalent ions (e.g., Ca^{2+}, Mg^{2+}) found in actual or simulated formation water. This controlled approach ensures that the fitting of the improved Carreau–Yasuda model strictly reflects the purely shear-dependent viscosity evolution. The coupled effects of salinity and formation water chemistry on the fluid's mechanical degradation represent a recognized limitation of the current model and will be a primary focus of our future optimization research.

To systematically evaluate the rheological properties, we prepared 10 different mass concentrations of the HPAM aqueous solution, ranging from 0.05 wt% to 0.50 wt% with an interval of 0.05 wt%. Following widely accepted international practices for enhanced oil recovery (EOR) fluid preparation [15,16], a specific mass of deionized water was accurately weighed in a 300 mL beaker. The sample was slowly added along the vortex wall over 30 s while switching on the digital slurry constant-speed stirrer at (400 ± 20) r/min, and

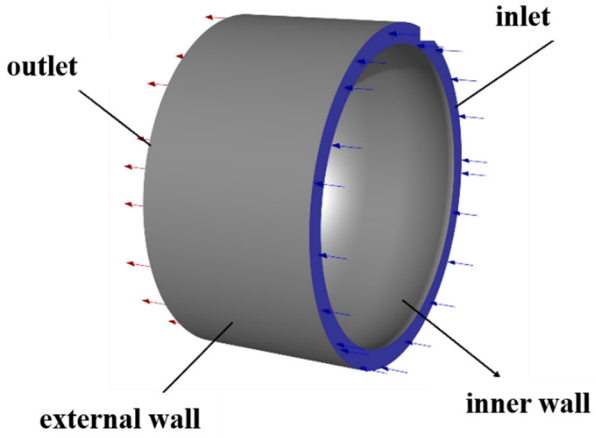
then stirred at (700 ± 20) r/min for 1 h [17]. The solution was allowed to stand for 24 h until the polyacrylamide was fully dissolved and the flow characteristics stabilized. The rheological tests were carried out in a Haake rotational rheometer (model Haake Mars60, Thermo Fisher Scientific, Waltham, MA, USA) with a double slit cylindrical rotor CC27 DG, with the shear rate varying linearly in the range of 0.1~10,000 s^{-1}. For each concentration, the rheometer recorded continuous data points across the entire shear rate sweep to ensure robust data fitting.

2.2. Geometric Model and Simulation Setup

Figure 1a illustrates the operational assembly of the injector, highlighting a narrow conduit known as the flow channel through which fluid is directed at the core of the device. Utilizing Solidworks software (Version 30.0, Dassault Systèmes, Vélizy-Villacoublay, France), a three-dimensional geometric model of the injector's flow channel has been crafted. The working cylinder, characterized by a diameter of 28.375 mm, is depicted in the model. A detailed view of the flow channel for an individual throttle unit is presented in Figure 1b, with the entire flow channel being composed of 16 such units. Upon completion of the geometric model, it is subsequently imported into the ANSYS Fluent 2022 R1 (Version 22.1, ANSYS, Inc., Canonsburg, PA, USA) workbench for mesh generation and computational fluid dynamics (CFD) analysis (Figure 2). As indicated in the flowchart (Figure 2), the "Adjust Mesh and Conditions" step refers to the essential iterative process of conducting grid independence tests and fine-tuning CFD solver settings (such as under-relaxation factors and near-wall treatments) to ensure the numerical pressure drop matches the physical loop experimental validation data within an acceptable error margin.



(**a**)



(**b**)

Figure 1. Geometry of the polymer injector: (**a**) 2D schematic with simulation region (blue dashed box) and high-pressure inlet; (**b**) 3D view of the assembly. The scale bar indicates 50 mm. The grey lines in (**a**) represent the housing structure.

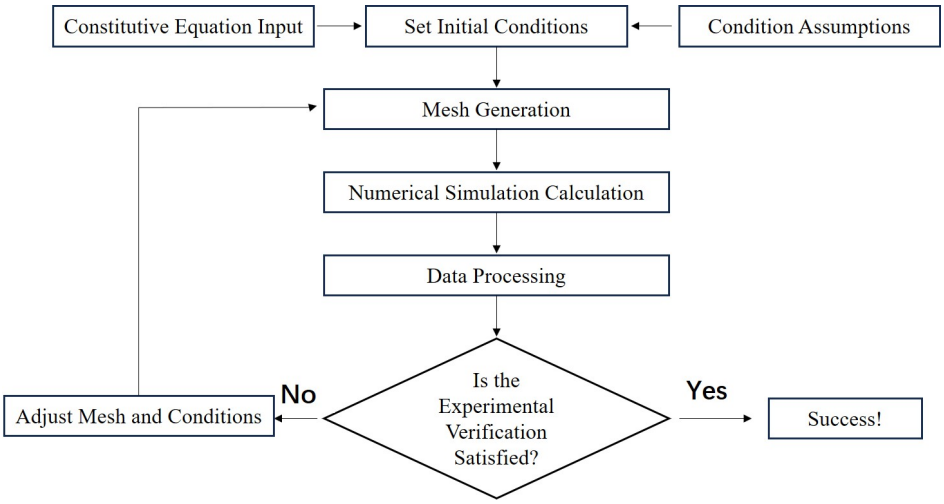


Figure 2. Flow Numerical Simulation Flowchart.

2.3. Numerical Simulation Method

To address the flow characteristics of non-Newtonian fluid within the polymer injector, the numerical simulation is conducted based on the following assumptions: (1) the fluid is incompressible with constant density; (2) the flow is steady-state, neglecting transient effects; and (3) heat transfer is neglected. The flow of the incompressible non-Newtonian fluid under isothermal conditions is governed by the continuity equation:

$$\nabla \cdot (\rho u) = 0 \tag{1}$$

and the Navier–Stokes momentum equations:

$$\rho(u \cdot \nabla) = -\nabla p + \nabla \cdot \tau \tag{2}$$

where ρ is the fluid density, u is the velocity vector, p is the static pressure, and τ is the extra stress tensor.

Given the high flow velocities of the polymer fluid (>10 m/s), the standard $k-\epsilon$ turbulence model was selected to effectively capture the turbulent flow field [18,19]. To accurately represent the physical flow loop, the computational domain was configured with a mass-flow inlet and a pressure outlet boundary condition. No-slip boundary conditions were applied to all solid walls. The numerical solution was achieved using the SIMPLEC algorithm for pressure–velocity coupling, with second-order upwind schemes for spatial discretization.

During the numerical simulation process, Fluent dynamically calculates the fluid viscosity based on the Carreau–Yasuda model defined in the User-Defined Function (UDF). This model was specifically chosen over the standard power-law model because the fluid in the injector transitions rapidly from a low-velocity Newtonian region to an extreme-shear throttling gap (>1000 s^{-1}). The Carreau–Yasuda model is uniquely capable of smoothly capturing both the zero-shear and infinite-shear viscosity plateaus at these extremes. The model characterizes the viscous behavior as follows:

$$\eta(\dot{\gamma}) = \eta_\infty + (\eta_0 - \eta_\infty)\left[1 + (\lambda\dot{\gamma})^a\right]^{\frac{n-1}{a}} \tag{3}$$

where η_0 is the zero-shear viscosity, η_∞ is the infinite-shear viscosity, λ is the relaxation time, n is the power-law index, and a is the Carreau constant [20–22]. It is critically important to note that polyacrylamide (HPAM) is a typical shear-thinning (pseudoplastic) fluid. There-

fore, its theoretical power-law index (n) must inherently be less than 1. Cases exhibiting a power-law index above 1 represent shear-thickening behavior, which contradicts the physical reality of the HPAM solution and were thus strictly excluded from this study. The viscosity retention rate was reconstructed using a weighted approach based on shear rate distribution.

To ensure the accuracy of the numerical results, a grid independence test was conducted. As shown in Figure 3, the total pressure drop stabilizes when the number of grid elements exceeds 1.5 million. Therefore, a mesh size of approximately 1.54 million elements was selected for all subsequent simulations.

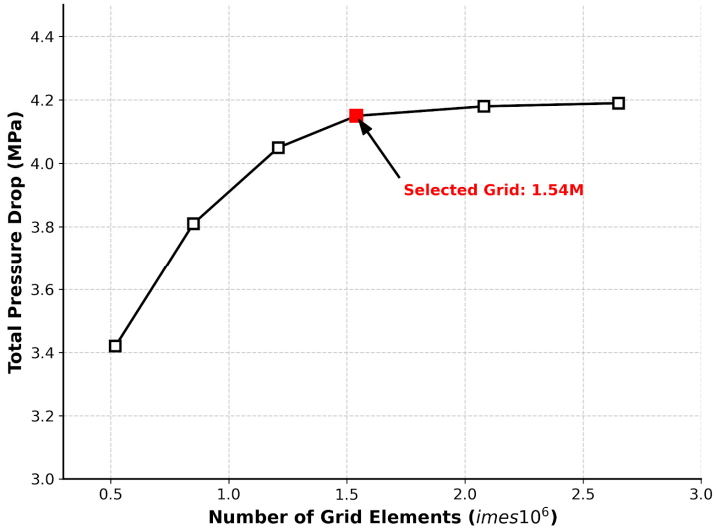


Figure 3. Grid independence test results.

3. Results and Discussion

3.1. Rheological Characteristics and Constitutive Equation

For polymeric fluids, viscosity is the most crucial parameter characterizing their viscous flow behavior. As shown in Figure 4, its rheological curve encompasses five distinct regions: the zero-shear plateau, the pseudoplastic region, the infinite-shear plateau, the viscoelastic region, and the degradation region. In the initial stage of shearing, the solution viscosity decreases rapidly ("shear thinning"). When the shear rate reaches approximately 7300 s^{-1}, the rheological properties undergo significant changes, identified as the critical shear rate [5,23,24].

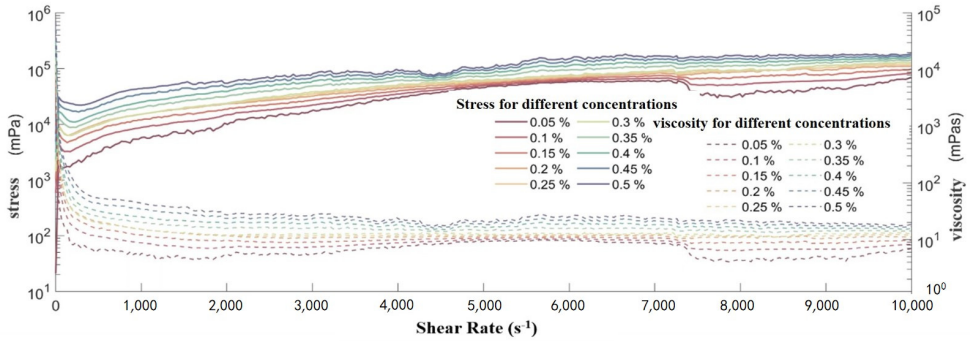


Figure 4. Variation curves of shear stress and viscosity with shear rate for aqueous solutions of different concentrations.

Based on the experimental data, the key parameters of the Carreau–Yasuda model (a, n, λ) were fitted using the least squares method (Table 1). The fitting accuracy (R^2) exceeded 0.977 and percentage errors were below 8.6% for all concentrations. As shown in Figure 5,

the regression curves exhibit excellent agreement with the experimental values (using 0.2 wt% concentration as a representative example), validating the model's applicability.

Table 1. Carreau–Yasuda model fitting results.

Mass Fraction (wt%)	Relaxation Time (λ)	a	n	Fitting Accuracy (R^2)	Percentage Error (%)
0.05	0.02156	0.006245	0.3264	0.9979	6.1
0.1	0.02204	0.008342	0.3499	0.9982	5.1
0.15	0.02578	0.01564	0.2515	0.9895	6.5
0.2	0.02794	0.01103	0.2560	0.9774	7.3
0.25	0.01964	0.01452	0.2123	0.9851	8.1
0.3	0.02097	0.01261	0.2883	0.9967	7.8
0.35	0.00921	0.1594	0.2434	0.9851	7.4
0.4	0.004072	0.1974	0.5045	0.9948	6.2
0.45	0.015611	0.2666	0.4256	0.9914	7.6
0.5	0.006026	0.1594	0.2739	0.9923	8.5

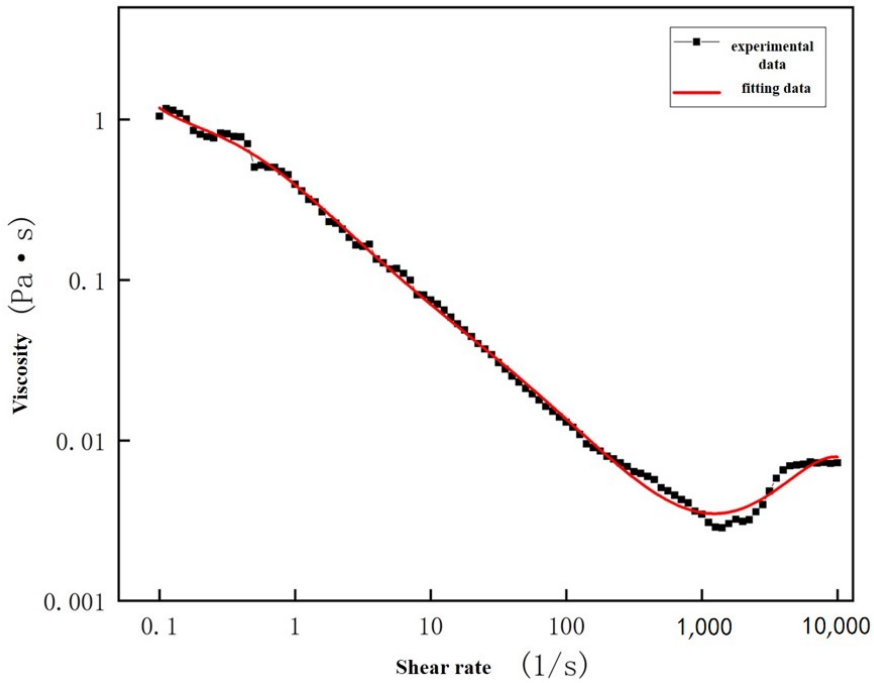


Figure 5. Comparison of experimental data and Carreau–Yasuda model fitting results for 0.2 wt% HPAM solution.

3.2. Model Verification

To verify the accuracy of the numerical model, a closed-loop flow experimental system was constructed. The HPAM solution was injected into the test section using a progressive cavity pump, specifically chosen to minimize initial shear degradation. High-precision pressure transmitters were installed immediately upstream and downstream of the test channel to record the differential pressure. In this study, Case 1 is defined as the physical model with a 129 mm clearance, and Case 2 corresponds to the model with a 94 mm clearance [6,7,10].

Verification was performed by comparing the simulated and measured pressure drops. Figure 6 illustrates the static pressure distribution contours for both cases. It is important to note that the negative pressure values displayed in the color scale (e.g., -3.58×10^3 Pa in Case 1) represent the gauge pressure relative to the reference operating pressure. As the fluid enters the narrow annular gap, the sudden cross-sectional contraction causes a drastic increase in flow velocity. According to Bernoulli's principle (the Venturi effect), this sharp increase in dynamic pressure leads to a corresponding drop in local static pressure.

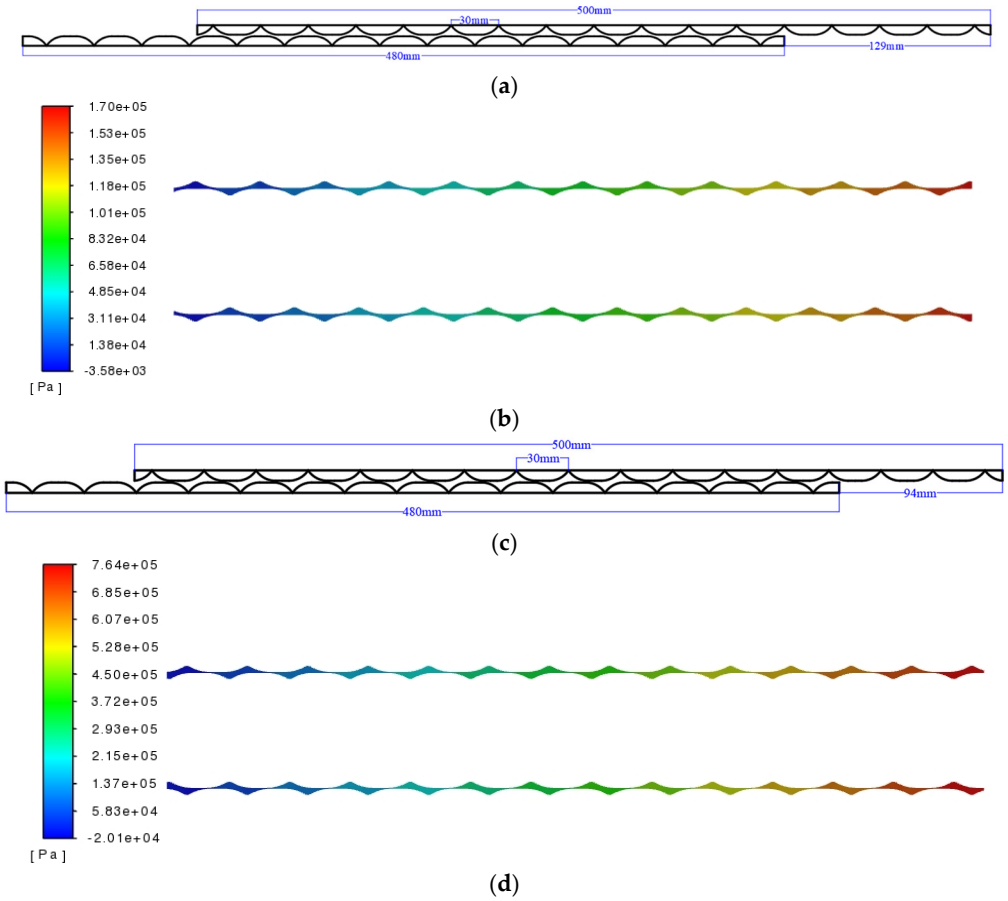


Figure 6. Experimental simulation comparison chart for working Case 1/2: (**a**) Case 1 fit dimension drawing; (**b**) Case 1 Pressure Distribution Contour; (**c**) Case 2 fit dimension drawing; (**d**) Case 2 Pressure Distribution Contour.

As shown in Table 2, for a 129 mm clearance, the simulated pressure drop deviated from the measured value by −0.03 MPa; for a 94 mm clearance, the deviation was +0.06 MPa. Under both conditions, deviations were within 15%, demonstrating that the established model correctly simulates the flow behavior and pressure drop variations.

Table 2. Specifications of the test section.

Groups	Volumes (m^3/d)	Pressure Drop (MPa)	Deviation (MPa)
Case 1 test	96	0.2	
Case 1 simulation	96	0.17	−0.03
Case 2 test	96	0.7	
Case 2 simulation	96	0.76	+0.06

3.3. Structural Optimization of Throttling Unit

This study systematically analyzed the influence of the upstream/downstream contour ratio and contour type on the throttling pressure drop. The dimensions for six optimization schemes are illustrated in Figure 7 (labeled Scheme I to Scheme VI). Note that although Scheme I and Scheme IV share the same D/L ratio of 20/30, the "streamlined" downstream profile in Scheme IV refers to a spline curve design intended to minimize abrupt flow separation compared to the linear profile.

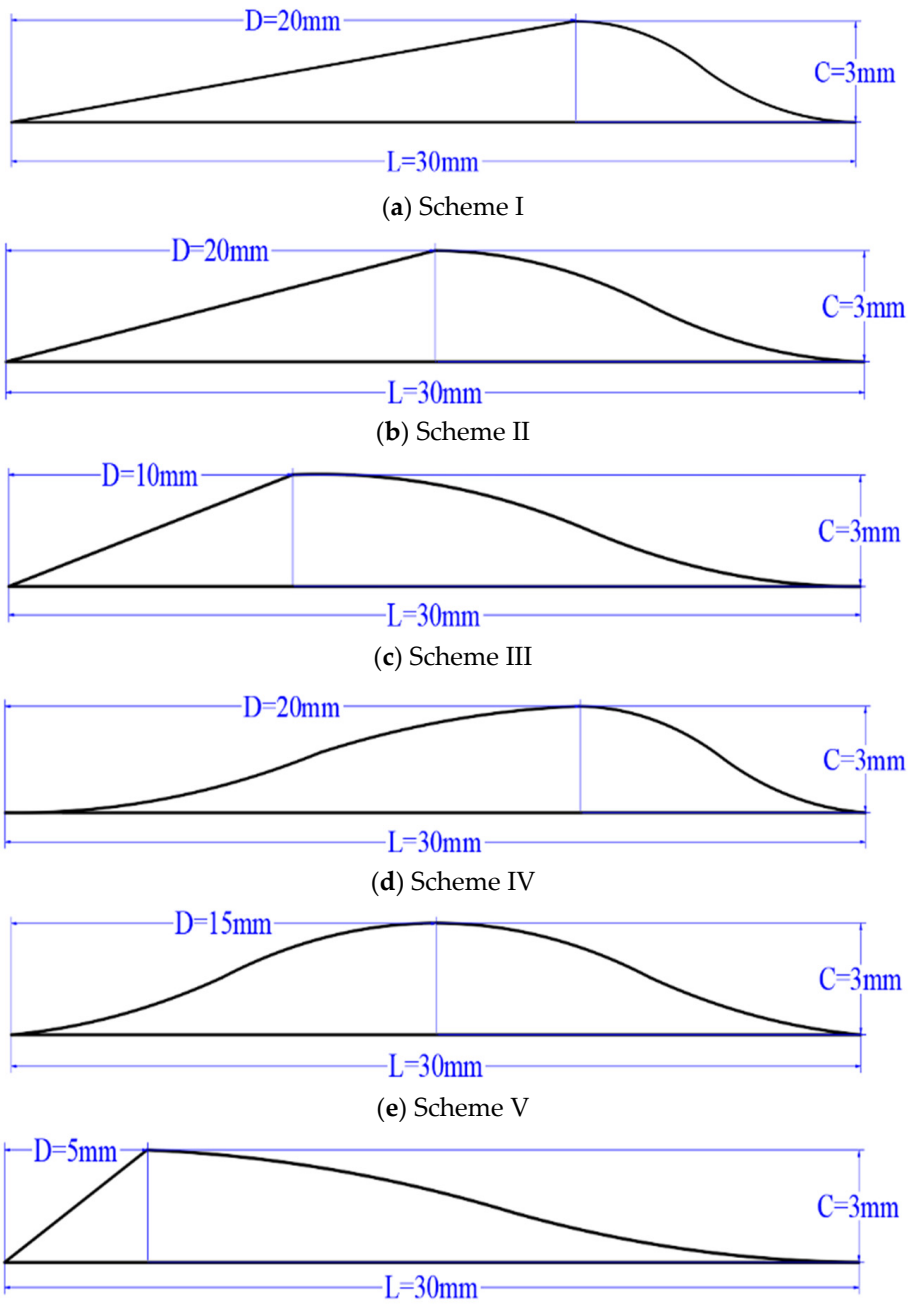


Figure 7. Schematic diagrams of six structural optimization schemes: (**a**) Scheme I (D/L = 20/30, Linear); (**b**) Scheme II (D/L = 15/30, Linear); (**c**) Scheme III (D/L = 10/30, Linear); (**d**) Scheme IV (D/L = 20/30, Streamline); (**e**) Scheme V (D/L = 15/30, Streamline); (**f**) Scheme VI (D/L = 5/30, Linear, Optimal Spindle-shaped Design).

The comprehensive working pressure drop data are visually compared in Figure 8.

To explain this, we analyzed the strain rate distribution. As shown in Figure 9, Scheme III generates a much larger high-shear zone at the throat entrance compared to Scheme I. The optimization of the downstream profile helps mitigate flow separation and stabilizes the boundary layer, a mechanism consistent with findings in other complex fluid systems [3,14,25,26].

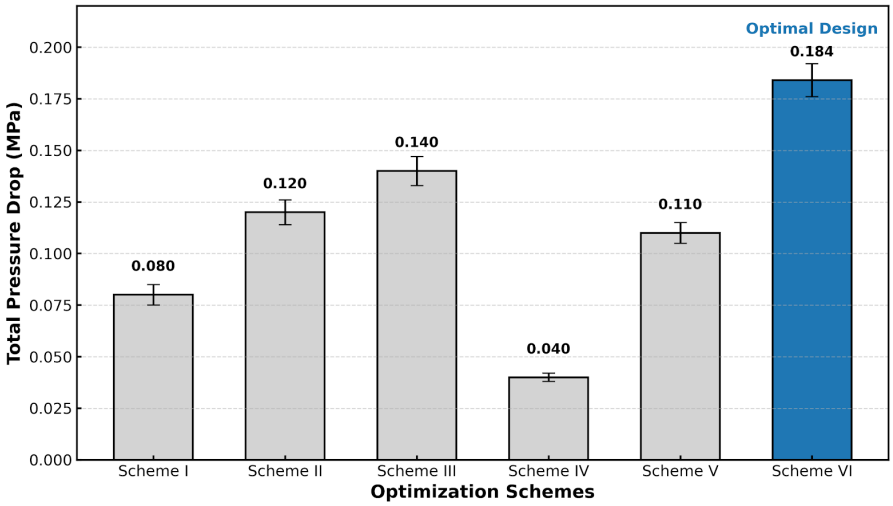
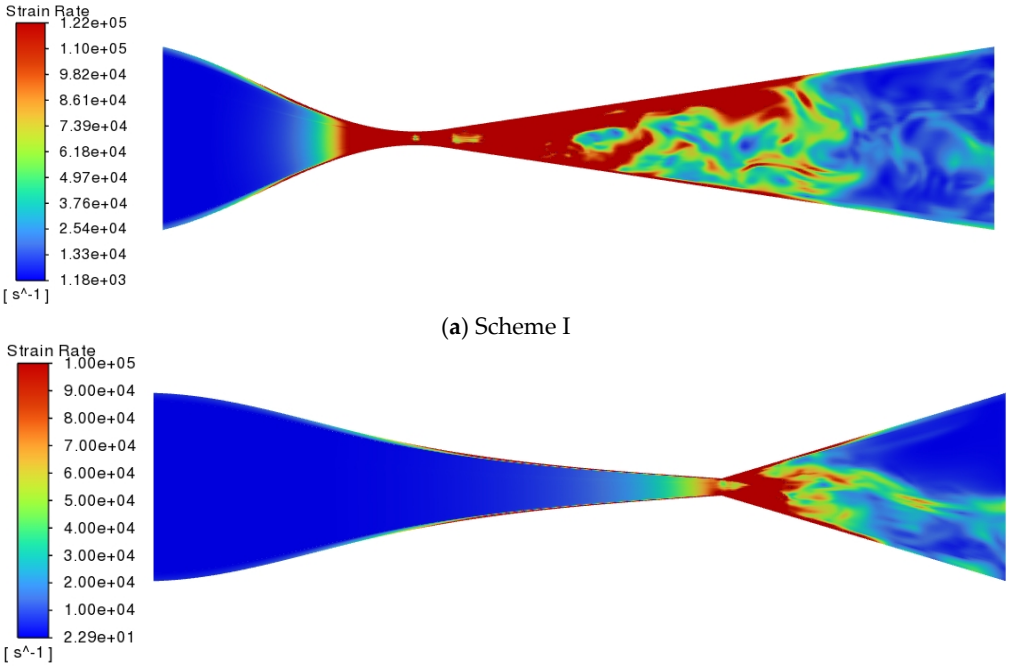


Figure 8. Comparison of total pressure drop across different optimization schemes. Scheme VI exhibits the highest pressure drop performance (0.184 MPa), significantly outperforming other designs.



(**a**) Scheme I

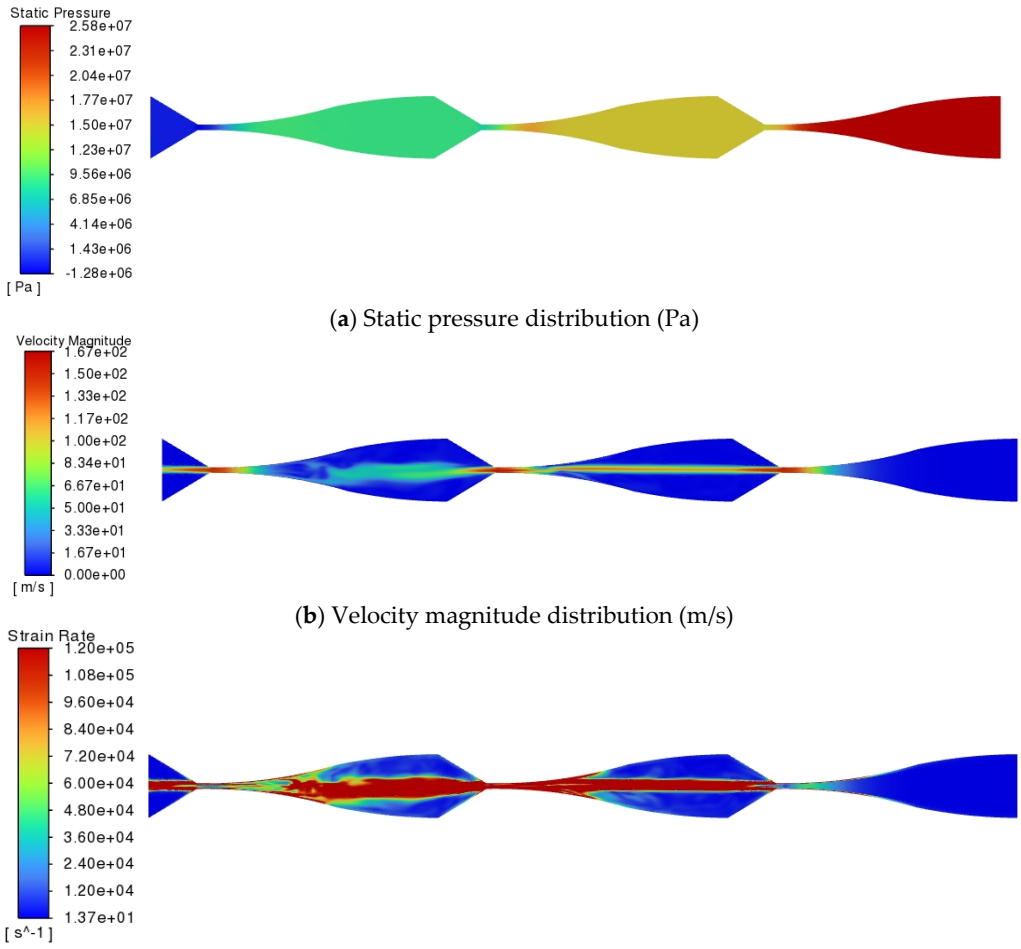
(**b**) Scheme III

Figure 9. Comparison of strain rate distribution contours (unit: s^{-1}) between: (**a**) Scheme I (Original Linear Design), showing high-shear regions (red) at the throat entrance; and (**b**) Scheme III, demonstrating a smoother flow transition and significantly reduced shear intensity.

The contour clearly shows that Scheme III generates a much larger high-shear zone at the throat entrance compared to Scheme I, leading to greater energy dissipation. Second, while a streamlined downstream design (Scheme IV) reduces shear intensity, it significantly weakens the pressure drop (50% decrease compared to Scheme I). This confirms that the linear downstream design (used in Schemes I, II, III, VI) plays a crucial compensatory role by maintaining necessary shear perturbation.

Based on these findings, a novel "spindle-shaped" optimization scheme (Scheme VI) was proposed. The detailed flow field of the optimal scheme, including the explicitly controlled shear rate distribution, is presented in Figure 10. Furthermore, the successful control of shear forces and pressure drop in Scheme VI demonstrates the potential applicability of

such geometric optimizations to other functional polymer systems, such as hydrogels and nanoparticle-enhanced fluids [27–30].



(**a**) Static pressure distribution (Pa)

(**b**) Velocity magnitude distribution (m/s)

(**c**) Shear rate distribution (s^{-1})

Figure 10. Local flow field distributions of the optimal Scheme VI (Spindle-shaped) showing 3 representative throttling units: (**a**) static pressure distribution (Pa); (**b**) velocity magnitude distribution (m/s); (**c**) shear rate distribution (s^{-1}).

The fundamental mechanism underlying the superior performance of the spindle-shaped design (Scheme VI) lies in its optimized spatial distribution of kinetic energy and strain rates(Table 3). Traditional linear designs typically force the fluid through an abrupt cross-sectional contraction, generating a highly localized, extreme-shear spike at the throat entrance that inevitably exceeds the critical shear rate for polymer chain scission. In contrast, the gradual upstream contraction in the spindle design pre-conditions the flow, distributing the velocity gradient more evenly over a longer axial distance. Subsequently, the controlled downstream expansion creates a stable flow separation zone that maximizes turbulent energy dissipation (contributing to the high pressure drop) without subjecting the bulk polymer chains to destructive mechanical forces.

When translating these findings to subsequent engineering optimizations, special attention must be paid to the coupled effects of bottom-hole temperature variations and multiphase flow conditions. Elevated temperatures in deep reservoirs may alter the polymer's relaxation time (λ) and shift the critical shear threshold, potentially requiring dynamic adjustments to the D/L ratio of the throttling unit. To visually summarize this flow mechanism, a conceptual schematic detailing the velocity gradient and polymer chain integrity within the optimized throttling unit is presented in Figure 11.

Table 3. Comparison data table of working pressure drop for six optimization schemes.

Schemes	Downstream Ratio D/L	Downstream Profile	Pressure Drop (MPa)
I	20:30	linear	0.08
II	15:30	linear	0.12
III	10:30	linear	0.14
IV	20:30	streamlined	0.04
V	15:30	streamlined	0.11
VI	5:30	linear	0.184

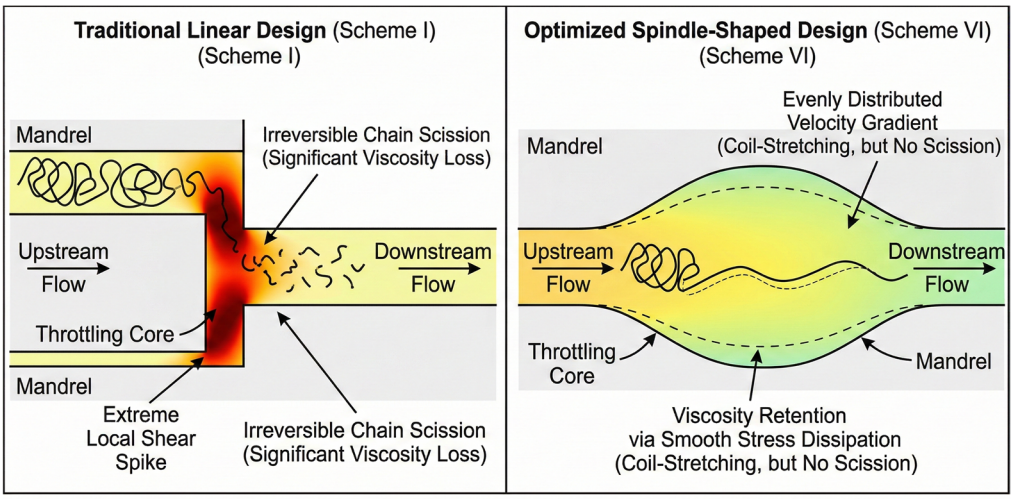


Figure 11. Conceptual schematic illustrating the mechanism of viscosity retention: comparison of highly localized shear and irreversible polymer chain scission in traditional abrupt contractions (left, Scheme I) versus evenly distributed velocity gradients and chain structural preservation in the optimized spindle-shaped design (right, Scheme VI).

4. Conclusions

(1) An improved Carreau–Yasuda viscosity constitutive model was established and validated. By incorporating the zero-shear and infinite-shear viscosity plateaus, this model accurately predicts the rheological behavior of HPAM solutions across a wide shear rate range (0.1–10,000 s^{-1}) with a prediction error of less than 8.6%, providing a reliable theoretical basis for injector simulation.

(2) Numerical optimization revealed the physical mechanism of the throttling unit: the upstream contraction ratio dominates the pressure drop generation by controlling the maximum velocity gradient, while the linear downstream profile is essential for maintaining shear perturbation to enhance energy dissipation.

(3) The novel spindle-shaped throttling unit (Scheme VI) resolves the conflict between high pressure drop and viscosity retention. Field applications confirm that the optimized injector achieves a 6.03 MPa pressure drop at 96 m^3/d (a 65% improvement over existing designs) while maintaining a viscosity retention rate above 85%. This design offers a robust solution for deep-well layered polymer injection in heterogeneous reservoirs.

Author Contributions: Methodology, J.M.; software, Y.Z. and X.Z.; validation, P.A.; formal analysis, Q.Q., C.R., X.Z. and Q.Z.; investigation, C.R.; resources, C.C.; data curation, Q.Q. and T.L.; writing—original draft, T.L.; writing—review and editing, Q.Z.; visualization, P.A.; supervision, J.M.; project administration, Y.Z. and C.C.; funding acquisition, T.L. All authors have read and agreed to the published version of the manuscript.

Funding: This research received no external funding.

Data Availability Statement: The original contributions presented in this study are included in the article. Further inquiries can be directed to the corresponding authors.

Conflicts of Interest: Qin Qian, Congkun Ren, Chuanrui Che, Xuemei Zhang and Jiaxing Ma were employed by SINOPEC Shengli Oilfield Company. The remaining authors declare that the research was conducted in the absence of any commercial or financial relationships that could be construed as a potential conflict of interest.

References

1. Seright, R.S.; Wang, D. Polymer flooding: Current status and future directions. *Pet. Sci.* **2023**, *20*, 1248–1259. [CrossRef]
2. Song, K.; Tao, J.; Li, X.; Xu, Y.; Liu, S. Recent Advances in Polymer Flooding in China. *Molecules* **2022**, *27*, 6978. [CrossRef] [PubMed]
3. Salem, K.G.; Tantawy, M.A.; Gawish, A.A.; Gomaa, S.; El-hoshoudy, A.N. Nanoparticles assisted polymer flooding: Comprehensive assessment and empirical correlation. *Geoenergy Sci. Eng.* **2023**, *226*, 211753. [CrossRef]
4. Sorbie, K.S. *Polymer-Improved Oil Recovery*; CRC Press: Boca Raton, FL, USA, 1991.
5. Standnes, D.C.; Skjevrak, I. Literature review of implemented polymer field projects. *J. Pet. Sci. Eng.* **2014**, *122*, 761–775. [CrossRef]
6. Zaitoun, A.; Makakou, P.; Blin, N.; Al-Maamari, R.S.; Al-Hashmi, A.R.; Abdel-Goad, M.; Al-Sharji, H.H. Shear stability of EOR polymers. *SPE J.* **2012**, *17*, 335–339. [CrossRef]
7. Jung, M.; Shakeri, P.; Seemann, R. Effect of viscoelasticity on displacement processes in porous media. *Front. Phys.* **2023**, *11*, 1099073. [CrossRef]
8. Husveg, T.; Stokka, M.; Jouenne, S.; Husveg, R. The Development of a Low-Shear Valve Suitable for Polymer Flooding. *SPE J.* **2020**, *25*, 2632–2647. [CrossRef]
9. Al Hashmi, A.R.; Al Maamari, R.S.; Al Shabibi, I.S.; Mansoor, A.M.; Zaitoun, A.; Al Sharji, H.H. Rheology and mechanical degradation of high-molecular-weight partially hydrolyzed polyacrylamide during flow through capillaries. *J. Pet. Sci. Eng.* **2013**, *105*, 100–106. [CrossRef]
10. Jouenne, S.; Chakibi, H.; Levitt, D. Polymer stability after successive mechanical-degradation events. *SPE J.* **2018**, *23*, 18–33. [CrossRef]
11. Morel, D.; Jouenne, S.; Vert, M.; Nahas, E. Polymer Injection in Deep Offshore Field: The Dalia Angola Case. In *SPE Annual Technical Conference and Exhibition*; Society of Petroleum Engineers: Houston, TX, USA, 2015. [CrossRef]
12. Bird, R.B.; Armstrong, R.C.; Hassager, O. *Dynamics of Polymeric Liquids, Volume 1: Fluid Mechanics*, 2nd ed.; Wiley-Interscience: New York, NY, USA, 1987.
13. Sochi, T. Non-Newtonian Flow in Porous Media. *Polymer* **2010**, *51*, 5007–5023. [CrossRef]
14. Salam, A.H.; Alsaif, B.; Hussain, S.M.S.; Khan, S.; Kamal, M.S.; Patil, S.; Al-Shalabi, E.W.; Hassan, A.M. Advances in Understanding Polymer Retention in Reservoir Rocks: A Comprehensive Review. *Polym. Rev.* **2024**, *211*, 1387–1413. [CrossRef]
15. Zhong, H.; Shi, B.; Bi, Y.; Shen, W.; Xu, Y.; Yin, H.; Xia, H.; Zhao, X. Flow mechanism of viscoelastic polymer flooding: State of the art review and outlook. *Chin. J. Theor. Appl. Mech.* **2024**, *56*, 847–861. [CrossRef]
16. Zhao, Y.; Dordzie, G.; Huh, C.; Balhoff, M.; Lu, Y. Rheology, Phase Stability, and Microstructure of Nanosilica-Assisted Partially Hydrolyzed Polyacrylamide. *Energy Fuels* **2024**, *38*, 2145–2158. [CrossRef]
17. Seright, R.S.; Fan, T.; Wavrik, K.; Balaban, R.C. New insights into polymer rheology in porous media. *SPE J.* **2011**, *16*, 35–42. [CrossRef]
18. Versteeg, H.K.; Malalasekera, W. *An Introduction to Computational Fluid Dynamics: The Finite Volume Method*, 2nd ed.; Pearson Education: Harlow, UK, 2007.
19. Launder, B.E.; Spalding, D.B. The numerical computation of turbulent flows. *Comput. Methods Appl. Mech. Eng.* **1974**, *3*, 269–289. [CrossRef]
20. Yasuda, K.; Armstrong, R.C.; Cohen, R.E. Shear flow properties of concentrated solutions of linear and star branched polystyrenes. *Rheol. Acta* **1981**, *20*, 163–178. [CrossRef]
21. Morrison, F.A. *Understanding Rheology*; Oxford University Press: New York, NY, USA, 2001.
22. Macosko, C.W. *Rheology: Principles, Measurements, and Applications*; Wiley-VCH: New York, NY, USA, 1994.
23. Zhang, H.; Lou, T.; Wang, X. Synthesis and properties of xanthan gum-acrylamide-carboxymethyl cellulose ternary anionic flocculants. *J. Water Process Eng.* **2023**, *53*, 104455. [CrossRef]
24. He, W.; Luo, J.; Wu, Y.; Luo, T.; Tang, C. Differently charged polyacrylamides (PAMs) significantly affect adsorption affinity and associated floc growth behaviors. *Sep. Purif. Technol.* **2023**, *329*, 125279. [CrossRef]
25. Grabsch, A.F.; Fawell, P.D.; Davies, M.G. Flocculating fine cuttings particles suspended within partially hydrolysed polyacrylamide (PHPA) solutions. *Miner. Eng.* **2024**, *206*, 108510. [CrossRef]

26. Al-Shakry, B.; Skauge, T.; Shaker Shiran, B.; Skauge, A. Impact of Mechanical Degradation on Polymer Injectivity in Porous Media. *Polymers* **2018**, *10*, 742. [CrossRef]
27. Husveg, R.; Stokka, M.; Husveg, T.; Albustin, R.; Jouenne, S. Field Testing a Low Shear Valve Suitable for Polymer Flooding in a Mother Solution Injection Scheme. In *Proceedings of the IOR 2021—21st European Symposium on Improved Oil Recovery, Vienna, Austria, 19–22 April 2021*; European Association of Geoscientists & Engineers (EAGE): Houten, The Netherlands, 2021. [CrossRef]
28. Åsen, S.M.; Stavland, A.; Strand, D.; Hiorth, A. An Experimental Investigation of Polymer Mechanical Degradation at cm and m Scale. In Proceedings of the SPE Improved Oil Recovery Conference, Tulsa, OK, USA, 14–18 April 2018. [CrossRef]
29. Huang, B.-Q.; Cui, H.-G.; Feng, T.-Y.; Yuan, C.-L.; Chang, A.-L.; Shao, M.-L.; Zhu, C.-F. Thin film composite polyamide nanofiltration membranes with interlayer constructed with core-shell structured polystyrene-polyacrylamide nanospheres. *J. Water Process Eng.* **2022**, *48*, 104844. [CrossRef]
30. Su, Z.; Xue, B.; Xu, C.; Dong, X. Mussel-Inspired Calcium Alginate/Polyacrylamide Dual Network Hydrogel. *Polymers* **2023**, *15*, 4498. [CrossRef]

Disclaimer/Publisher's Note: The statements, opinions and data contained in all publications are solely those of the individual author(s) and contributor(s) and not of MDPI and/or the editor(s). MDPI and/or the editor(s) disclaim responsibility for any injury to people or property resulting from any ideas, methods, instructions or products referred to in the content.